Transient Natural Convection of a Chemically Reactive Fluid in a Vertical Annulus under the Combined Influence of Heat Source/Sink and Soret Effect

Sylvester Bakut Joseph
Department of Mathematics and Statistics, Nuhu Bamalli Polytechnic, Zaria, Nigeria

Abstract
This paper investigates transient natural convection flow of a chemically reactive fluid in a vertical annulus, considering the combined influence of heat source/sink and Soret diffusion. The governing conservation equations are treated using a semi-analytical method, and the resulting solutions are expressed in modified Bessel functions. The analysis predicts that internal heat generation enhances fluid velocity and thermal gradients, while heat absorption promotes faster stabilization of the flow field. The Soret effect introduces strong coupling between temperature and concentration, significantly influencing mass transfer and buoyancy-driven circulation. These interactions modify the Nusselt and Sherwood numbers, as well as skin-friction characteristics across the annular region. The study provides practical relevance to systems such as catalytic reactors, geothermal exchangers, and energy devices where coupled heat–mass transport under reactive conditions plays a critical role.

Keywords: Thermal diffusion; Riemann-sum approximation; concentric cylinders; mass transfer; heat transfer

Nomenclature:

C' - Dimensional fluid concentration (kg/m^3)
C_p - Specific heat capacity (J/kgK)
D_c - Coefficient of mass diffusion (m^2/s)
D_t - Coefficient thermal diffusion (m^2/s)
g - Acceleration due to gravity(m/s^2)
K^* - Chemical reaction $(1/s)$
Q_0 - Heat generation / absorption coefficient (J)
r' - Radial coordinate (m)
Sh - Sherwood number
St - Soret number
t' - Time (s)
T' - Fluid temperature (K)
u' - Velocity(m/s)

Greek symbols:

α - Thermal diffusion coefficient(m^2/s)
β_t - Coefficient of thermal expansion $(1/K)$
β_c - Mass expansion coefficient(m^3/kg)
ς_1 - Inner pipe radius (m)
ς_2 - Outer pipe radius (m)
ν - Kinematic viscosity(m^2/s)
ρ - Fluid density(kg/m^3)
τ - Skin-friction

Introduction:

Flows in vertical annular domains have remained a focus of transport phenomena research because of their prevalence in advanced thermal systems, ranging from compact heat exchangers and geothermal wells to nuclear reactor cooling and porous insulation designs. Unlike simple channels or single cylinders, annuli generate distinctive buoyancy-driven behavior owing to their curvature and dual boundary surfaces. These features strongly influence how velocity, temperature, and concentration fields evolve, especially when the system is subjected to additional physical processes such as volumetric heating or cooling, chemical reactions, and cross-diffusion effects. Investigating these combined influences under transient conditions is essential for capturing the dynamic interplay between momentum,

https://doi.org/10.5281/zenodo.17252181

heat, and mass transfer that cannot be reduced to steady-state approximations.

A significant body of research has highlighted the role of internal heat generation or absorption in annular convection. These terms arise naturally in contexts such as exothermic chemical processes, nuclear waste canisters, and radiative absorption in participating media. Heat generation intensifies buoyancy, increases local fluid temperatures, and accelerates convective motion, while absorption removes thermal energy, tending to suppress instabilities and smooth gradients (Anurag, 2021; Jha &Aina, 2018). Studies have shown that even small volumetric source or sink terms can alter the transient approach to equilibrium, changing peak wall temperatures and modifying velocity fields before stabilization occurs (Oni & Jha, 2019; Dwivedi et al., 2023). These findings are highly relevant for safety-critical operations such as nuclear cooling and reactive processing.

Superimposed on this are cross-diffusion phenomena, particularly the Soret effect, where a temperature gradient induces mass flux. In multicomponent or reactive fluids, this thermal diffusion mechanism redistributes chemical species, often enhancing concentration gradients in regions of strong heating. The result is a modified buoyancy force, which couples solutal and thermal fields in nontrivial ways (Jha, et al, 2015). Raji and Bessaïh (2022) reported that the simultaneous action of Soret and Dufour effects in annular ducts leads to asymmetric convection patterns and oscillatory transitions, which are absent in purely Fickian transport. In porous annuli, Sankar, et al. (2012) found that thermal diffusion amplifies solutal transport during the early transient stages, delaying homogenization and extending the unsteady regime. Such findings indicate that ignoring cross-diffusion can lead to underestimation of transient instabilities in coupled systems.

Chemical reactions further complicate the physics. Endothermic and exothermic reactions not only consume or release heat but also alter concentration fields, thereby modifying buoyancy and momentum transfer. Analytical studies by Jha, et al (2013) demonstrated that the inclusion of reaction kinetics in vertical annuli leads to significant departures in the time evolution of velocity and concentration, even for moderate reaction rates. Roy, et al (2019) similarly found that reactive effects shift both Nusselt and Sherwood numbers, reshaping the overall transport efficiency. These results suggest that when chemical activity and thermal diffusion act together, the path to steady state is governed by a delicate balance between heat release, mass redistribution, and momentum exchange.

Transient analysis is particularly critical because most real systems do not operate under constant conditions. Processes such as reactor startups, periodic wall heating, and chemical dosing occur on time scales where unsteady dynamics cannot be ignored. Gambo and Gambo (2021) showed that magnetically influenced annular flows under internal heating evolve through transient regimes that control operational safety margins, while Muhammad et al. (2024) demonstrated experimentally that time-dependent heat absorption in iso-flux heated annuli substantially reduces maximum wall temperatures. These observations underscore that the transient period, far from being a minor prelude, often governs peak stresses and determines system reliability.

Computational and experimental studies have broadened understanding by probing parameter regimes beyond analytical reach. Dutta, et al (2022) employed higher-order schemes to capture double-diffusive instabilities in annuli and reported that transient flow structures could be suppressed or amplified depending on diffusivity ratios. Chtaibi et al. (2024) extended the analysis to non-Newtonian fluids in magnetohydrodynamic fields, revealing that the interplay of rheology and thermal diffusion leads to new instability modes. Experimental work by Cadena-de la Peña, et al (2017) confirmed that nanofluid-filled annuli exhibit transient behaviors heavily influenced by volumetric heating, validating theoretical predictions. Similarly, Zhang, et al (2021)

https://doi.org/10.5281/zenodo.17252181

showed numerically that nanofluid-filled porous annuli exhibit enhanced convection patterns, but these remain highly sensitive to internal heat sources. Together, these works illustrate the need for models that integrate multiple transport effects rather than treating them in isolation.

The practical implications of such findings are broad. In nuclear waste management, porous annular barriers must dissipate long-term volumetric heating while remaining chemically stable (Jha, et al, 2016). In chemical reactors, controlling thermal runaway requires precise understanding of how transient heating couples with reactive and diffusive mechanisms (Taiwo, 2017). Enhanced oil recovery processes involve in-situ combustion, where reactive fluids flow through annular porous structures under both heat release and thermal diffusion. Even compact electronic cooling systems exploit annular geometries where transient startup effects can determine stress levels on sensitive components (Chen, et al, 2010). Across these domains, accurate transient modeling is indispensable.

Yet, while significant progress has been made, the literature reveals a gap. Most studies emphasize either the role of heat generation, or Soret-driven diffusion, or chemical reactivity, but rarely all together in transient annular settings. For example, Ojemeri, et al (2023) examined Soret and magnetic field effects on reactive annular flows, while Anurag (2021) focused on volumetric heating under Newtonian conditions. Only a few studies attempt to combine multiple effects simultaneously, and even fewer address the complete interplay of transient natural convection, internal heat source/sink, Soret diffusion, and chemical reaction. This lack of integrated treatment limits predictive accuracy for Multiphysics environments where all of these mechanisms coexist.

To address this, semi-analytical approaches are particularly useful. Methods based on Laplace transforms and modified Bessel functions have proven effective for cylindrical geometries, enabling exact or approximate solutions that satisfy boundary conditions rigorously (Oni & Jha, 2019). These solutions not only serve as benchmarks for numerical simulations but also clarify the roles of key nondimensional parameters such as the heat generation parameter, chemical reaction rate, Soret number, and buoyancy ratio. By systematically analyzing their influence, it becomes possible to identify parameter ranges that enhance or suppress transient instabilities, informing the design of more efficient and safer systems.

In light of these observations, the transient natural convection of chemically reactive fluids in vertical annuli under the combined action of heat source/sink and Soret effects represents an important but underexplored research direction. It links thermal-fluid sciences with chemical kinetics and multicomponent diffusion in a geometry of direct industrial relevance. A comprehensive analysis of this coupled system will provide new insights into the temporal development of flow, heat, and mass transfer, filling a critical gap in the literature and offering valuable benchmarks for complex engineering applications.

1. Mathematical analysis

The unsteady natural convection boundary-layer flow of an incompressible viscous fluid in an annulus formed by isothermal concentric tubes is considered. The radii of the inner and outer tubes are respectively $\varsigma_1$and $\varsigma_2$while the z'-axis is vertically upward in the direction of the axis of the tubes with the r'-axis perpendicular to it. The flow configuration of the problem is shown in Figure 1. For$t' \leq 0$, the temperature(T_0) and concentration(C_0) of the fluid and the walls of the tubes are equal. These are then raised or lowered to$T_w$and C_w at the wall of the inner tube for $t' > 0$with the temperature and concentration of the outer tube preserved at the ambient state. The following assumptions are taken into consideration:

i. The thermal fluxes influence the concentration fluxes,
ii. A temperature-dependent heat source/sink having the linear form $Q_0(T' - T_0)$ exists

https://doi.org/10.5281/zenodo.17252181

with $Q_0 < 0$depicting a heat source and $Q_0 > 0$ indicating a heat sink,

iii. The fluid experiences a first-order chemical reaction of the form $K^*(C' - C_0)$ where $K^* < 0$depicts a reaction that is generative with species being created and $K^* > 0$depicts a reaction that is destructive where species are destroyed,

iv. The flow is dependent on$r'$and t'as a result of being fully developed.

Applying the Boussinesq approximation and the no-slip condition, the dimensional flow model is:

$$\frac{\partial u'}{\partial t'} = \nu \frac{1}{r'}\frac{\partial}{\partial r'}\left(r'\frac{\partial u'}{\partial r'}\right) + g\beta_T(T' - T_0) + g\beta_C(C' - C_0) \quad (1)$$

$$\frac{\partial T'}{\partial t'} = \alpha \frac{1}{r'}\frac{\partial}{\partial r'}\left(r'\frac{\partial T'}{\partial r'}\right) + \frac{Q_o}{\rho C_p}(T' - T_0) \quad (2)$$

$$\frac{\partial C'}{\partial t'} = D_c \frac{1}{r'}\frac{\partial}{\partial r'}\left(r'\frac{\partial C'}{\partial r'}\right) + D_t \frac{1}{r'}\frac{\partial}{\partial r'}\left(r'\frac{\partial T'}{\partial r'}\right) - K^*(C' - C_0) \quad (3)$$

The initial $(t' \leq 0)$ conditions for this model are:

$$u' = 0, T' = T_0, C' = C_0, \text{ at } \varsigma_1 \leq r' \leq \varsigma_2 \quad (4)$$

The boundary $(t' > 0)$ conditions are given as:

$$u' = 0 \begin{cases} T' = T_w,\ C' = T_w \ \ at\ r' = \varsigma_1 \\ T' = T_0,\ \ C' = T_0\ at\ r' = \varsigma_2 \end{cases} \quad (5)$$

Consider the following dimensionless parameters:

$$\left.\begin{array}{c} r = \frac{r'}{\varsigma_1}, t = \frac{t'\nu}{{\varsigma_1}^2}, \theta = \frac{T'-T_0}{T_w-T_0}, \mathrm{u} = \frac{\nu u'}{g{\varsigma_1}^2\beta_t(T_w-T_0)}, \\ \phi = \frac{C'-C}{C_w-C_0}, \mathrm{St} = \frac{D_t(T_w-T_0)}{D_c(C_w-C_0)}, K = \frac{K^*{\varsigma_1}^2}{\nu},\ \mathrm{H} = \frac{Q_0{\varsigma_1}^2}{\nu\rho C_p} \end{array}\right\} \quad (6)$$

Using equation (6), the dimensional governing equations (1)-(3) are rendered non-dimensional and are presented as:

$$\frac{\partial u}{\partial t} = \frac{1}{r}\frac{\partial}{\partial r}\left(r\frac{\partial u}{\partial r}\right) + \theta + \mathrm{N}\phi \quad (7)$$

$$\frac{\partial \theta}{\partial t} = \frac{1}{Pr}\frac{1}{r}\frac{\partial}{\partial r}\left(t\frac{\partial \theta}{\partial r}\right) - H\theta \quad (8)$$

$$\frac{\partial \phi}{\partial t} = \frac{1}{Sc}\left[\frac{1}{r}\frac{\partial}{\partial r}\left(r\frac{\partial \phi}{\partial r}\right) + St\frac{1}{r}\frac{\partial}{\partial r}\left(r\frac{\partial \theta}{\partial r}\right)\right] - K\phi \quad (9)$$

In equations (7)-(9), $\mathrm{Pr} = \nu/\alpha$is the Prandtl number,$\mathrm{Sc} = \upsilon/D$ is the Schmidt number, and $\mathrm{N} = \beta_c(C_w - C_0)/\beta_t(T_w - T_0)$ is the buoyancy ratio.

Initial $(t \leq 0)$ conditionsare presented as:

$$u = 0, \theta = 0, \phi = 0, \text{ at } 1 \leq r \leq \lambda \quad (10)$$

Boundary $(t > 0)$ conditionsare given as:

$$u = 0 \begin{cases} \theta = 1, \phi = 1 \ \ at\ r = 1 \\ \theta = 0, \phi = 0 \ \ at\ r = \lambda \end{cases} \quad (11)$$

where$\lambda = \frac{\varsigma_1}{\varsigma_2}$, is the radii ratio.

Let $\bar{F}(r,s) = \int_0^\infty F(r,t)e^{-pt}dt$ be a function defining the Laplace transforms of$u, \theta,$ andϕ. Then, the governing equations (7) - (9) with initial condition (10) reduce to the following:

$$\frac{1}{r}\frac{d}{dr}\left(r\frac{d\bar{u}}{dr}\right) - s\bar{u} = -\bar{\theta} - \mathrm{N}\bar{\phi} \quad (12)$$

$$\frac{1}{r}\frac{d}{dr}\left(r\frac{d\bar{\theta}}{dr}\right) - \mathrm{Pr}\,(s + H)\bar{\theta} = 0 \quad (13)$$

$$\frac{1}{r}\frac{d}{dr}\left(r\frac{d\bar{\phi}}{dr}\right) + St\frac{1}{r}\frac{d}{dr}\left(r\frac{d\bar{\theta}}{dr}\right) - \mathrm{Sc}\,(s + K)\bar{\phi} = 0 \quad (14)$$

From equations (13) and (14), we have

$$\frac{1}{r}\frac{d}{dr}\left(r\frac{d\bar{\phi}}{dr}\right) + St\mathrm{Pr}\,(s + H)\bar{\theta} - \mathrm{Sc}\,(s + K)\bar{\phi} = 0 \quad (15)$$

The boundary condition (11) becomes

$$\bar{u} = 0 \begin{cases} \bar{\theta} = \frac{1}{p}, \bar{\phi} = \frac{1}{p} \ \ at\ r = 1 \\ \bar{\theta} = 0, \bar{\phi} = 0 \ \ at\ r = \lambda \end{cases} \quad (16)$$

https://doi.org/10.5281/zenodo.17252181

Solutions:

Let $a_1 = \Pr(s+H)$ and $a_2 = \mathrm{Sc}(s+K)$. The solution to Equation (13) is

$$\bar{\theta}(r,s) = \frac{K_0(\lambda\sqrt{a_1})I_0(r\sqrt{a_1}) - K_0(r\sqrt{a_1})I_0(\lambda\sqrt{a_1})}{s[K_0(\lambda\sqrt{a_1})I_0(\sqrt{a_1}) - K_0(\sqrt{a_1})I_0(\lambda\sqrt{a_1})]} \quad (17)$$

By using equation (17) in (15), the solution for the concentration is

$$\bar{\phi}(r,s) = \left(1 + \frac{a_1 St}{a_1 - a_2}\right)\frac{K_0(\lambda\sqrt{a_2})I_0(r\sqrt{a_2}) - I_0(\lambda\sqrt{a_2})K_0(r\sqrt{a_2})}{s[K_0(\lambda\sqrt{a_2})I_0(\sqrt{a_2}) - K_0(\sqrt{a_2})I_0(\lambda\sqrt{a_2})]} - \frac{a_1 St}{s(a_1 - a_2)}\frac{K_0(\lambda\sqrt{a_1})I_0(r\sqrt{a_1}) - I(\lambda\sqrt{a_1})K_0(r\sqrt{a_1})}{K_0(\lambda\sqrt{a_1})I_0(\sqrt{a_1}) - K_0(\sqrt{a_1})I_0(\lambda\sqrt{a_1})} \quad (18)$$

Again, using equations (17) and (18) in (12), the solution for the velocity is

$$\bar{u}(r,s) = \left(\frac{1}{s(a_1 - s)}\left(1 - \frac{Na_1 St}{a_1 - a_2}\right) + \frac{N}{s(a_2 - s)}\left(1 + \frac{a_1 St}{a_1 - a_2}\right)\right)\frac{K_0(\lambda\sqrt{p})I_0(r\sqrt{p}) - I_0(\lambda\sqrt{p})K_0(r\sqrt{p})}{K_0(\lambda\sqrt{p})I_0(\sqrt{p}) - K_0(\sqrt{p})I_0(\lambda\sqrt{p})} - \frac{1}{s(a_1 - p)}\left(1 - \frac{Na_1 St}{a_1 - a_2}\right)\frac{K_0(\lambda\sqrt{a_1})I_0(r\sqrt{a_1}) - I(\lambda\sqrt{a_1})K_0(r\sqrt{a_1})}{K_0(\lambda\sqrt{a_1})I_0(\sqrt{a_1}) - K_0(\sqrt{a_1})I_0(\lambda\sqrt{a_1})} - \frac{N}{s(a_2 - s)}\left(1 + \frac{a_1 St}{a_1 - a_2}\right)\frac{K_0(\lambda\sqrt{a_2})I_0(r\sqrt{a_2}) - I_0(\lambda\sqrt{a_2})K_0(r\sqrt{a_2})}{K_0(\lambda\sqrt{a_2})I_0(\sqrt{a_2}) - K_0(\sqrt{a_2})I_0(\lambda\sqrt{a_2})} \quad (19)$$

From equations (17)-(19), the Nusselt and Sherwood numbers and the skin friction are respectively given as:

$$\overline{\mathrm{Nu}} = -\left.\frac{d\bar{\theta}}{d\varsigma}\right|_{r=1,\lambda} = \frac{\sqrt{a_1}[K_0(\lambda\sqrt{a_1})I_1(r\sqrt{a_1}) + K_1(r\sqrt{a_1})I_0(\lambda\sqrt{a_1})]}{s[K_0(\lambda\sqrt{a_1})I_0(\sqrt{a_1}) - K_0(\sqrt{a_1})I_0(\lambda\sqrt{a_1})]} \quad (20)$$

$$\overline{Sh} = -\left.\frac{d\bar{\phi}}{d\varsigma}\right|_{r=1,\lambda} = \left(1 + \frac{a_1 St}{a_1 - a_2}\right)\frac{K_0(\lambda\sqrt{a_2})I_0(r\sqrt{a_2}) - I_0(\lambda\sqrt{a_2})K_0(r\sqrt{a_2})}{s[K_0(\lambda\sqrt{a_2})I_0(\sqrt{a_2}) - K_0(\sqrt{a_2})I_0(\lambda\sqrt{a_2})]} - \frac{a_1 St}{s(a_1 - a_2)}\frac{K_0(\lambda\sqrt{a_1})I_0(r\sqrt{a_1}) - I(\lambda\sqrt{a_1})K_0(r\sqrt{a_1})}{K_0(\lambda\sqrt{a_1})I_0(\sqrt{a_1}) - K_0(\sqrt{a_1})I_0(\lambda\sqrt{a_1})} \quad (21)$$

$$\bar{\tau} = \left.\frac{d\bar{u}}{dr}\right|_{r=1} = \sqrt{s}\left(\frac{1}{s(a_1 - s)}\left(1 - \frac{Na_1 St}{a_1 - a_2}\right) + \frac{N}{s(a_2 - s)}\left(1 + \frac{a_1 St}{a_1 - a_2}\right)\right)\frac{K_0(\lambda\sqrt{s})I_1(\sqrt{s}) + I_0(\lambda\sqrt{s})K_1(\sqrt{s})}{[K_0(\lambda\sqrt{s})I_0(\sqrt{s}) - K_0(\sqrt{s})I_0(\lambda\sqrt{s})]} - \frac{\sqrt{a_1}}{s(a_1 - s)}\left(1 - \frac{Na_1 St}{a_1 - a_2}\right)\frac{K_0(\lambda\sqrt{a_1})I_1(\sqrt{a_1}) + I_0(\lambda\sqrt{a_1})K_1(\sqrt{a_1})}{K_0(\lambda\sqrt{a_1})I_0(\sqrt{a_1}) - K_0(\sqrt{a_1})I_0(\lambda\sqrt{a_1})} - \frac{N\sqrt{a_2}}{s(a_2 - s)}\left(1 + \frac{a_1 St}{a_1 - a_2}\right)\frac{K_0(\lambda\sqrt{a_2})I_1(\sqrt{a_2}) + I_0(\lambda\sqrt{a_2})K_1(\sqrt{a_2})}{[K_0(\lambda\sqrt{a_2})I_0(\sqrt{a_2}) - K_0(\sqrt{a_2})I_0(\lambda\sqrt{a_2})]} \quad (22)$$

$$\bar{\tau} = -\left.\frac{d\bar{u}}{d\varsigma}\right|_{r=\lambda} = \sqrt{s}\left(\frac{1}{s(a_1 - s)}\left(1 - \frac{Na_1 St}{a_1 - a_2}\right) + \frac{N}{s(a_2 - s)}\left(1 + \frac{a_1 St}{a_1 - a_2}\right)\right)\frac{K_0(\lambda\sqrt{s})I_1(\lambda\sqrt{s}) + I_0(\lambda\sqrt{s})K_1(\lambda\sqrt{s})}{s[K_0(\lambda\sqrt{s})I_0(\sqrt{s}) - K_0(\sqrt{s})I_0(\lambda\sqrt{s})]} - \frac{\sqrt{a_1}}{p(a_1 - s)}\left(1 - \frac{Na_1 St}{a_1 - a_2}\right)\frac{K_0(\lambda\sqrt{a_1})I_1(\lambda\sqrt{a_1}) + I_0(\lambda\sqrt{a_1})K_1(\lambda\sqrt{a_1})}{K_0(\lambda\sqrt{a_1})I_0(\sqrt{a_1}) - K_0(\sqrt{a_1})I_0(\lambda\sqrt{a_1})} - \frac{N\sqrt{a_2}}{s(a_2 - s)}\left(1 + \frac{a_1 St}{a_1 - a_2}\right)\frac{K_0(\lambda\sqrt{a_2})I_1(\lambda\sqrt{a_2}) + I_0(\lambda\sqrt{a_2})K_1(\lambda\sqrt{a_2})}{s[K_0(\lambda\sqrt{a_2})I_0(\sqrt{a_2}) - K_0(\sqrt{a_2})I_0(\lambda\sqrt{a_2})]} \quad (23)$$

1.1. Inversion of the Laplace transform:

The inversion of Equations (17) - (22) is required and is obtained by

$$\Lambda(r,t) = \frac{e^{\varepsilon t}}{t}\left[\frac{1}{2}\bar{\Lambda}(r,\varepsilon) + Re\sum_{k=1}^{N}\bar{\Lambda}\left(r, \varepsilon + \frac{ik\pi}{t}\right)(-1)^k\right] \quad (24)$$

Equation (23) is the Riemann sum approximation method used for the inversion. Here, replacing Λ byu, θ, ϕ, Nu, Sh,and τ in equations (17)-(22) yield their respective inversion.

1.2. Validation of solutions:

https://doi.org/10.5281/zenodo.17252181

Validation of the computer routine of the numerical procedure of the Riemann sum approximation method (RSA) for the velocity profiles is carried out for the case of steady-state flowby setting $\partial/\partial t$ in equations (7)-(9) to zero and solving to give the velocity as:

$$u(r) = \left(1-\frac{\ln r}{\ln \lambda}\right)\left(\frac{1}{{a_1}^*}\left(1-\frac{N{a_1}^*St}{{a_1}^*-{a_2}^*}\right)+\frac{N}{{a_2}^*}\left(1+\frac{{a_1}^*St}{{a_1}^*-{a_2}^*}\right)\right)- \frac{1}{{a_1}^*}\left(1-\frac{N{a_1}^*St}{{a_1}^*-{a_2}^*}\right)\frac{K_0(\lambda\sqrt{{a_1}^*})I_0(r\sqrt{{a_1}^*})-I_0(\lambda\sqrt{{a_1}^*})K_0(r\sqrt{{a_1}^*})}{K_0(\lambda\sqrt{{a_1}^*})I_0(\sqrt{{a_1}^*})-I_0(\lambda\sqrt{{a_1}^*})K_0(\sqrt{{a_1}^*})}- \frac{N}{{a_2}^*}\left(1+\frac{{a_1}^*St}{{a_1}^*-{a_2}^*}\right)\frac{K_0(\lambda\sqrt{{a_2}^*})I_0(r\sqrt{{a_2}^*})-I_0(\lambda\sqrt{{a_2}^*})K_0(r\sqrt{{a_2}^*})}{K_0(\lambda\sqrt{{a_2}^*})I_0(\sqrt{{a_2}^*})-I_0(\lambda\sqrt{{a_2}^*})K_0(\sqrt{{a_2}^*})}. \quad (25)$$

where ${a_1}^* = HPr$ and ${a_2}^* = KSc$.

Furthermore, a Matlab PDEPE numerical solution is presented comparatively with the results of this article and the numerical values of the exact solution (ES) of equation (25) in Table 1.

Results and Discussion:

Figures 1 through 10 and Tables 1 and 2 illustrate the impact of heat sinks ($H > 0$), destructive chemical reactions ($K > 0$), and critical dimensionless parameters on transient natural convection occurring within a vertical annulus.

Temperature Field

Figure 1 shows that steep initial temperature gradients gradually relax toward steady-state conditions as time progresses. A larger radius ratio impedes heat penetration, consequently delaying thermal equilibration. In Figure 2, it is evident that elevated Prandtl numbers confine heat to the inner wall, resulting in sharper gradients and thinner thermal layers, while lower Prandtl numbers facilitate broader diffusion. The presence of a heat sink further lowers the fluid temperature; under conditions of high heat absorption, penetration becomes so restricted that the outer wall remains unaffected.

Concentration Field

The solute transport process evolves more slowly than temperature changes. As illustrated in Figure 3, concentration levels progress toward a steady state but require extended durations in wider gaps due to increased diffusion distances. Figure 4 indicates that destructive reactions diminish solute concentrations, while the Soret effect induces thermally driven mass flux; the interplay between these mechanisms determines the strength of stratification. Figure 5 reveals that, although the heat sink predominantly influences heat transfer, it also affects the Soret-driven accumulation of solute. High values of the parameter intensify stratification despite the presence of the sink, while lower values yield nearly uniform concentration profiles. Figure 6 confirms that an increase in the Schmidt number reduces mass diffusivity, leading to steeper gradients and higher Sherwood numbers. In contrast, lower Schmidt numbers promote mixing and result in flatter concentration profiles.

Velocity Field

The evolution of velocity corresponds with the development of buoyancy forces. Figure 7 exhibits acceleration during the initial phases, followed by a transition to steady velocity profiles; a larger parameter redistributes buoyancy and postpones the attainment of velocity peaks. Figure 8 emphasizes that destructive reactions weaken solutal buoyancy and reduce velocity, whereas the Soret effect enhances coupling and shifts the locations of velocity maxima. In Figure 9, high values of the examined parameter confine buoyancy near the wall, resulting in increased shear while suppressing core flow, whereas low values diffuse buoyancy and enhance convection. The heat sink reduces velocities in both scenarios. Figure 10 demonstrates that higher values of the analyzed parameter maintain solutal gradients, resulting in stronger buoyancy and larger velocities, while lower values encourage mixing and produce weaker flow patterns.

Heat and Mass Transfer Characteristics

https://doi.org/10.5281/zenodo.17252181

Table 1 presents an analysis of the Nusselt number, showing an increase at the inner wall as the system transitions from a transient to a steady state. Concurrently, the Sherwood numbers and skin friction demonstrate systematic variations concerning the Prandtl number (Pr), Stanton number (St), Schmidt number (Sc), heat transfer coefficient (H), and thermal conductivity (K). Enhanced buoyancy conditions significantly improve both heat and mass transfer, with the heat sink and destructive reactions influencing their interplay. The accuracy of the numerical method is validated by Table 2, which illustrates that the Riemann sum approximation aligns with the embedded partial differential equation problem (PDEPE) to the third decimal place, converging to precise steady-state values.

Conclusion:

This study clarifies that both the heat sink and destructive reactions effectively suppress the temperature, concentration, and velocity fields within a vertical annulus. In contrast, the Soret effect alleviates these reductions by promoting solutal buoyancy. Elevated heat conditions confine thermal energy near the inner wall, while significant solutal stratification is maintained under high conditions, delaying the equilibration process across the gap. To accurately predict convection behaviors in such systems, it is essential to consider the combined influences of thermal and solutal diffusion, cross-diffusion, and chemical reactions. The validation of the Riemann sum method confirms its effectiveness in capturing transient behaviors. The insights gained from this study have direct applications in engineering contexts involving reactive fluids, as well as in thermal management for internal heating or cooling applications and annular geometries.

References:

Anurag S.., Singh, A. K., Chandran, P., & Sacheti, N. C. (2021). Effect of Newtonian heating/cooling on free convection in an annular permeable region in the presence of heat source/sink. Heat Transfer, 50(4), 3562–3586. https://doi.org/10.1002/htj.21900

Cadena-de la Peña, N. L., Mota-Babiloni, A., Navarro-Esbrí, J., & Sánchez, D. (2017). Experimental analysis of natural convection in vertical annuli filled with nanofluids. International Journal of Thermal Sciences, 117, 276–286. https://www.sciencedirect.com/science/article/abs/pii/S1290072915300612

Chen, S., Tölke, J., &Krafczyk, M. (2010). Numerical investigation of double-diffusive natural convection in vertical annuluses with opposing temperature and concentration gradients. International Journal of Heat and Fluid Flow, 31(2), 217–226. https://www.sciencedirect.com/science/article/abs/pii/S0142727X10000093

Chtaibi, K., Dahani, Y., Amahmid, A., Hasnaoui, M., & Ben Hamed, H. (2024). Numerical simulation of combined effects of a vertical magnetic field and thermal radiation on natural convection of non-Newtonian fluids confined between circular and square concentric cylinders. Journal of the Taiwan Institute of Chemical Engineers, 161, 105538. https://doi.org/10.1016/j.jtice.2024.105538

Dutta, S., Chatterjee, D., & Halder, P. (2022). Heat and mass transfer characteristics of double-diffusive natural convection in a vertical annulus using a higher-order compact scheme. Heat Transfer, 51(8), 6974–6995. https://doi.org/10.1002/htj.22300

Dwivedi, N., Singh, A. K., & Sacheti, N. C. (2023). Influence of temperature-dependent heat source/sink on MHD transient free convection in a vertical concentric annulus. International Communications in Heat and Mass Transfer, 146, 106991. https://doi.org/10.1016/j.icheatmasstransfer.2023.106991

Gambo, J. J., & Gambo, D. (2021). On the effect of heat generation/absorption on fully developed natural convection in an open-ended vertical concentric annulus under a magnetic field. Heat Transfer. https://doi.org/10.1002/htj.21978

Jha, B. K., &Aina, B. (2018). Investigation of heat generation/absorption on natural convection flow in a vertical annular micro-

channel: An exact solution. Multidiscipline Modeling in Materials and Structures, 14(1), 143–167. https://doi.org/10.1108/MMMS-06-2017-0056

Jha, B. K., & Oni, M. O. (2019). Natural convection flow in a vertical annulus with time-periodic thermal boundary conditions. Propulsion and Power Research, 8(1), 43–55. https://doi.org/10.1016/j.jppr.2018.12.002

Jha, B. K., Aina, B., & Oni, M. O. (2016). Steady fully developed mixed convection flow in a vertical micro-concentric annulus with heat generating/absorbing fluid: An exact solution. Ain Shams Engineering Journal, 7(4), 1199–1209. https://www.academia.edu/33472405

Jha, B. K., Joseph, S. B., &Ajibade, A. O. (2015). Role of thermal diffusion (Soret effect) on double-diffusive natural convection in a vertical annular porous medium. Ain Shams Engineering Journal, 6(2), 629–637. https://doi.org/10.1016/j.asej.2014.11.004

Jha, B. K., Samaila, A. K., &Ajibade, A. O. (2013). Unsteady/steady natural convection flow of reactive viscous fluid in a vertical annulus. International Journal of Applied Mechanics and Engineering, 18(1), 73–83. https://doi.org/10.2478/ijame-2013-0005

Muhammad, Y. M., Lawan, M. A., &Gambo, Y. Y. (2024). Influence of heat absorption on MHD natural convection in vertical concentric annuli. Nigerian Journal of Science and Technical Research, 6(2), Article 1313. https://journals.nipes.org/index.php/njstr/article/view/1313

Ojemeri, G., Abdulsalam, S., & Ahmad, S. K. (2023). Influence of Soret and radial magnetic field on natural convection of a chemically reactive fluid in a vertical porous annulus. UMYU Scientifica, 2(3), 108–120. https://pdfs.semanticscholar.org/c3c4/75ccab94dd2a95c37daebfd303d8d28d7f2b.pdf

Oni, M. O., & Jha, B. K. (2019). Heat generation/absorption effect on natural convection flow in a vertical annulus with time-periodic boundary conditions. Journal of Aircraft and Spacecraft Technology, 3(1), 183–196. https://doi.org/10.3844/jastsp.2019.183.196

Raji, A., &Bessaïh, R. (2022). Natural convection process in a coaxial (annular) duct with Soret and Dufour effects. International Journal of Numerical Methods for Heat & Fluid Flow, 33(1), 96–119. https://doi.org/10.1108/HFF-02-2022-0106

Roy, N. C., Hossain, A., & Gorla, R. S. R. (2019). Natural convective flow of a chemically reacting fluid in an annulus. Heat Transfer—Asian Research, 48(4), 1345–1369. https://doi.org/10.1002/htj.21435

Sankar, M., Shivakumara, I. S., &Venkatachalappa, M. (2012). Double-diffusive convection from a discrete heat and solute source in a vertical porous annulus. Transport in Porous Media, 92(1), 81–98. https://doi.org/10.1007/s11242-011-9871-1

Taiwo, Y. S. (2017). Exact solution of an MHD natural convection flow in vertical concentric annulus with heat absorption. International Journal of Fluid Mechanics & Thermal Sciences, 3(5), 52–61. https://doi.org/10.11648/j.ijfmts.20170305.12

Zhang, L., Zhou, L., & Shao, X. (2021). Numerical study of natural convection heat transfer in a porous annulus filled with a Cu nanofluid. Nanomaterials, 11(4), 1037. https://www.ncbi.nlm.nih.gov/pmc/articles/PMC8070222/

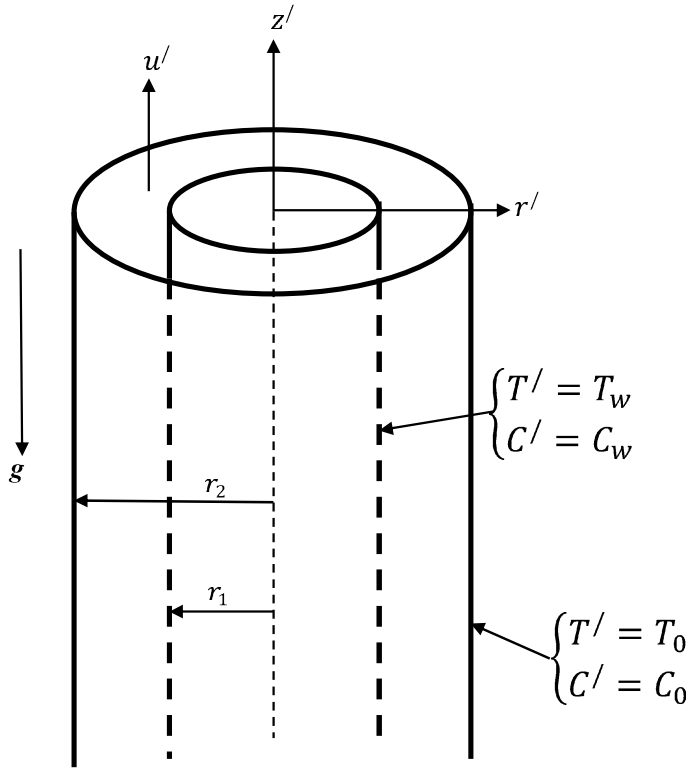

Figure 1: Vertical annulus with constant wall boundary conditions

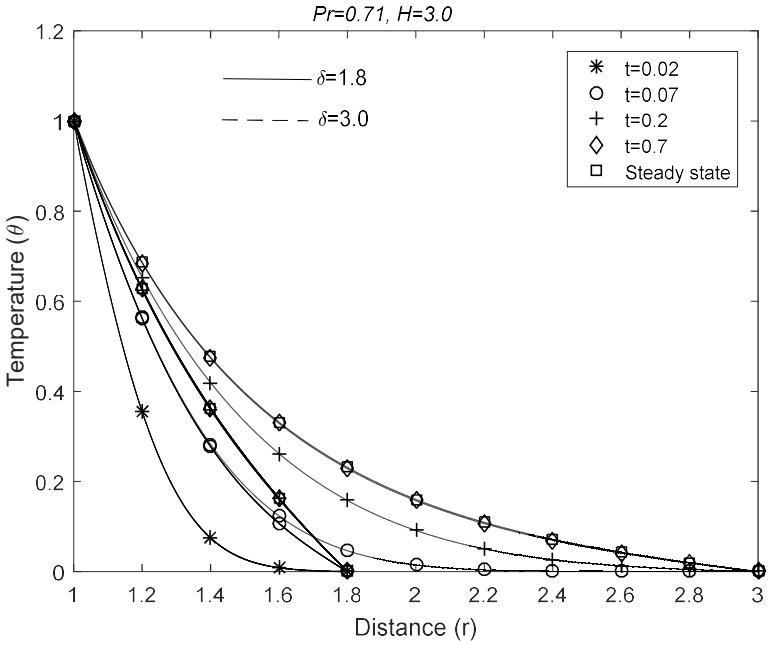

Figure 2: Effect of time and radii ratio on temperature profiles

https://doi.org/10.5281/zenodo.17252181

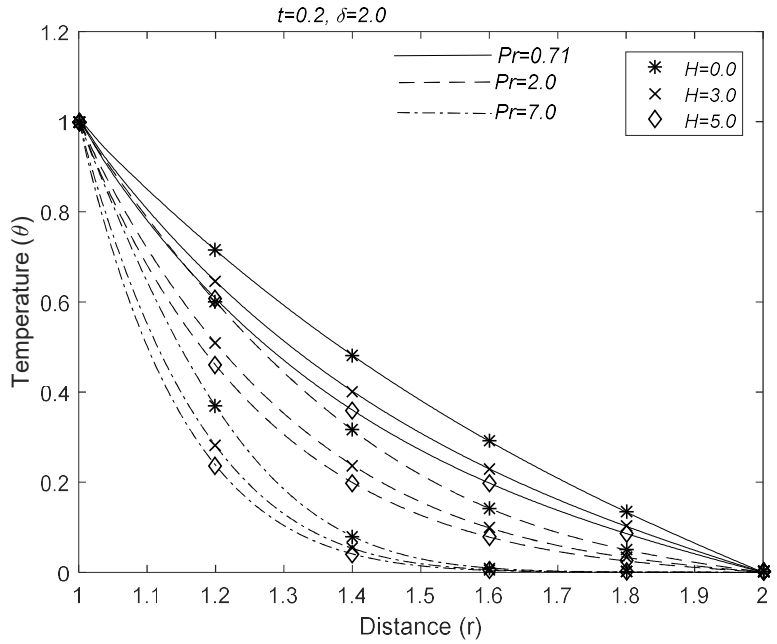

Figure 3: Effect of Prandtl number and heat sink on the temperature profiles

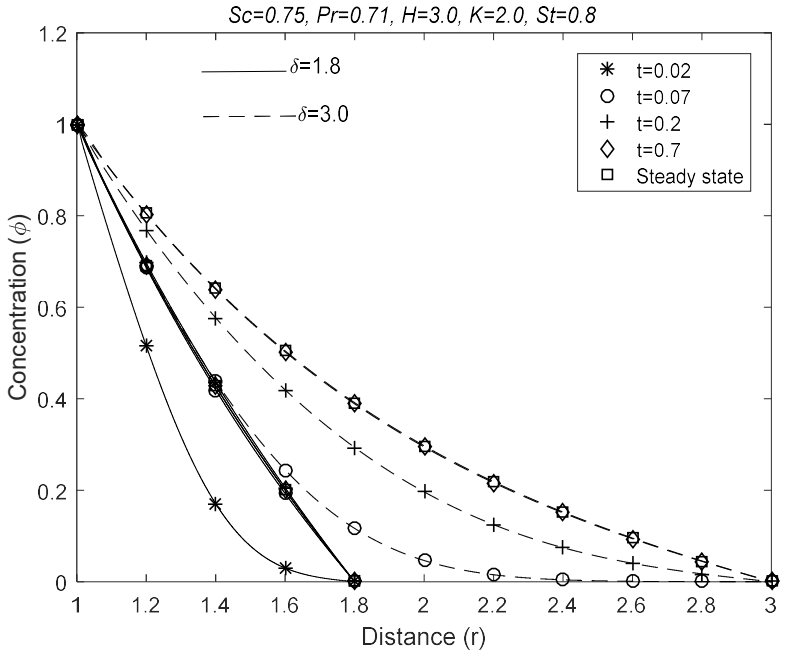

Figure 4: Effect of time and radii ratio on concentration profiles

https://doi.org/10.5281/zenodo.17252181

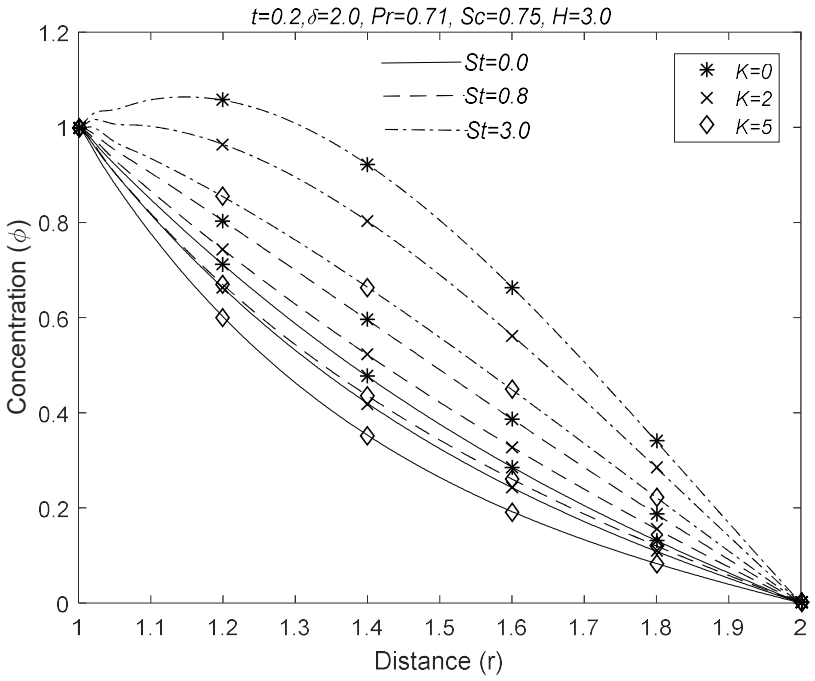

Figure 5: Effect of Soret number and destructive chemical reaction on the concentration profiles

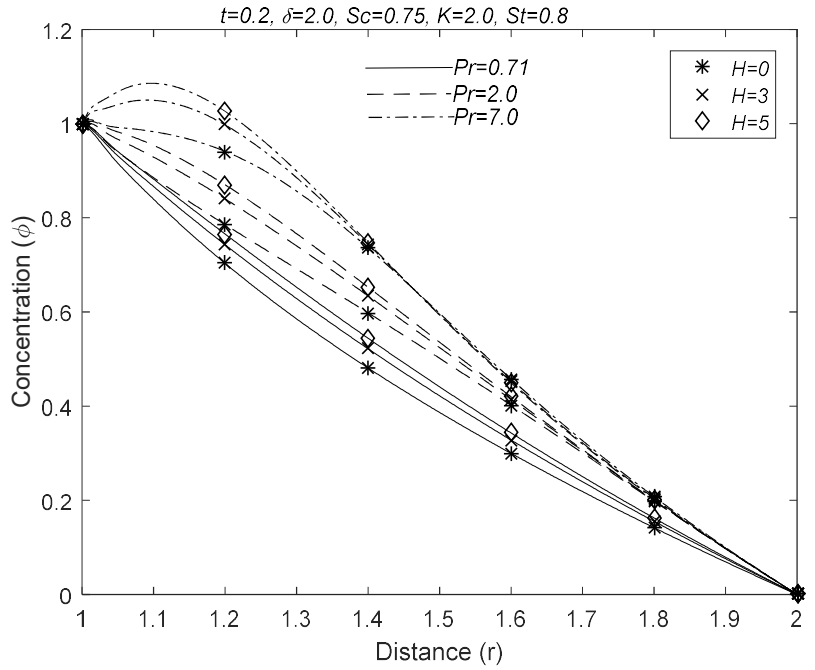

Figure 6: Effect of Prandtl number and heat sink on the concentration profiles

https://doi.org/10.5281/zenodo.17252181

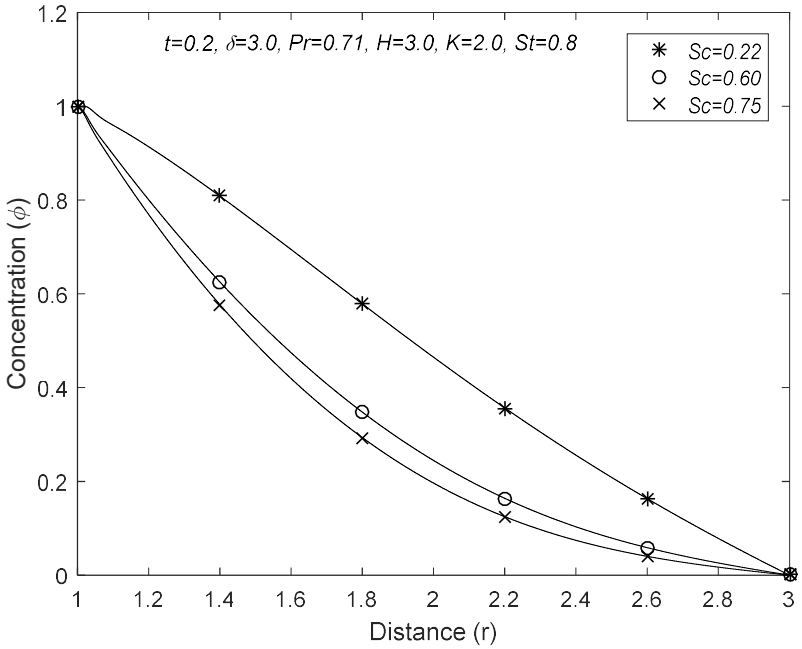

Figure 7: Effect of Schmidt number on the concentration profiles

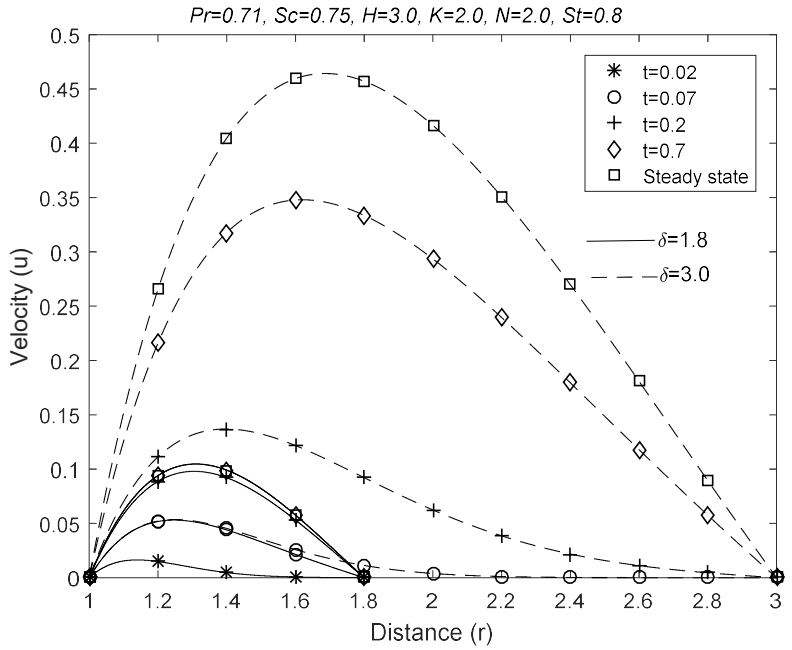

Figure 8: Effect of time and radii ratio on the velocity profiles

https://doi.org/10.5281/zenodo.17252181

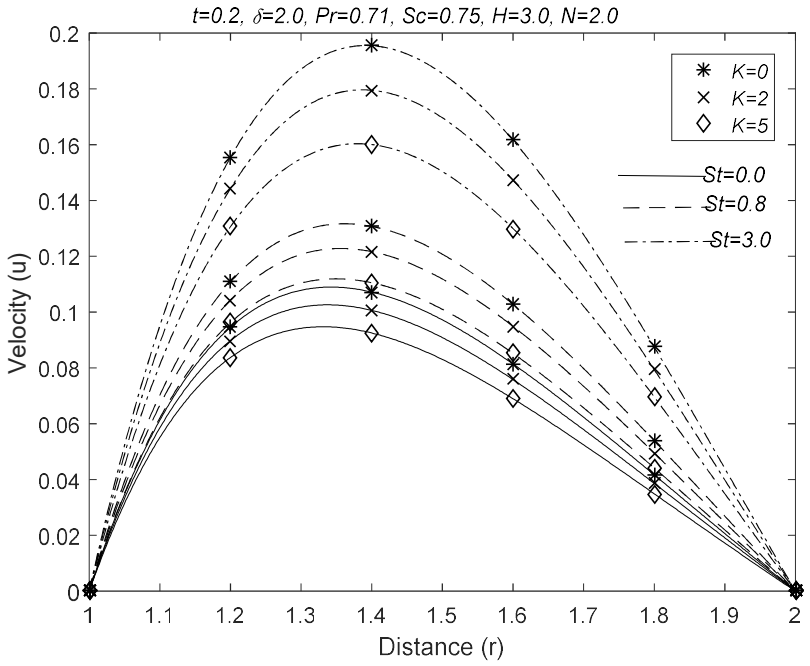

Figure 9: Effect of destructive reaction and Soret number on the velocity profiles

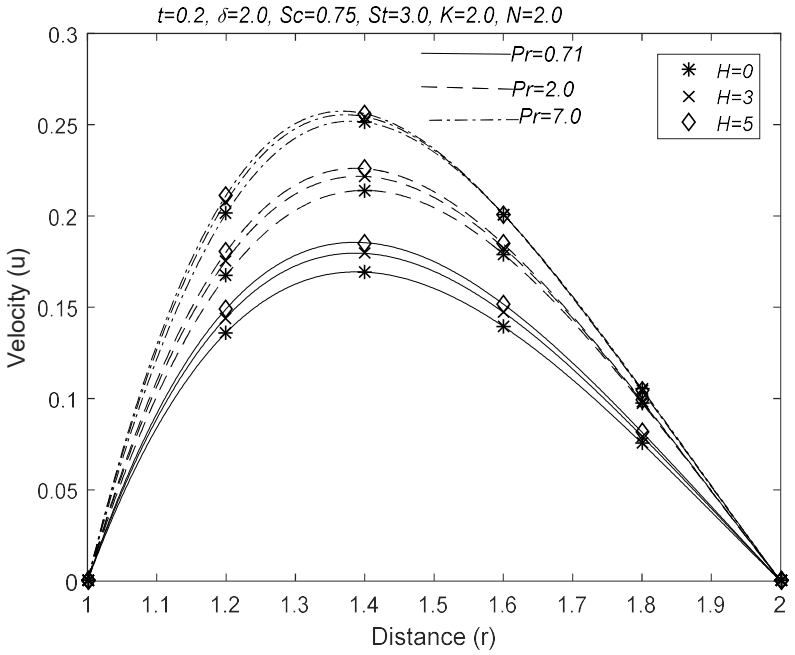

Figure 10: Effect of Prandtl number and heat sink on the velocity profiles

https://doi.org/10.5281/zenodo.17252181

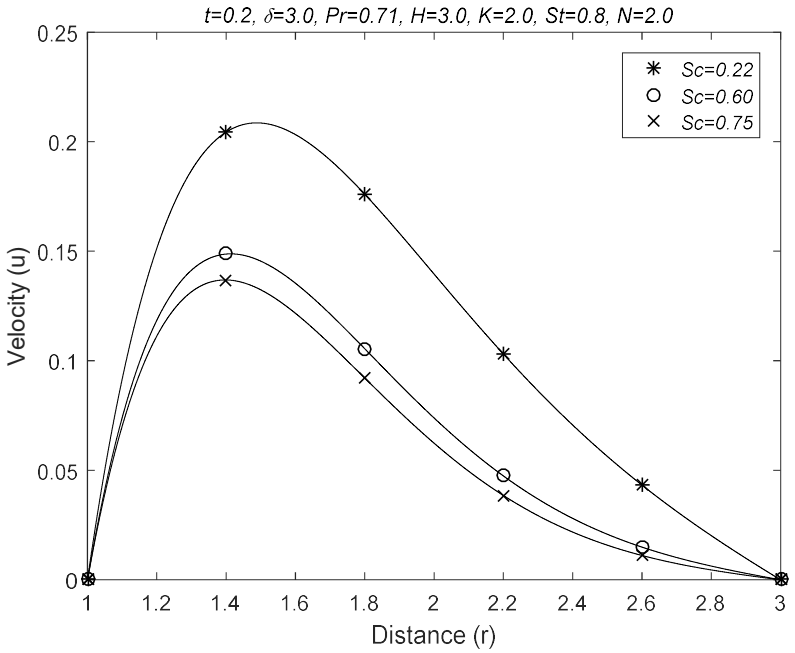

Figure 11: Effect of Schmidt number on the velocity profiles

Table 1: Nusselt number, Sherwood number and Skin-friction at the walls of the annulus for different flow parameters ($Pr = 0.71, Sc = 0.60, K = 2.0, H = 3.0, N = 2.0, St = 0.2, t = 0.2, \delta = 2.0, r = 1.5$

		Nu		*Sh*		τ	
		r=1	r=δ	r=1	r=δ	r=1	r=δ
t	0.07	1.1565	0.0295	0.2906	0.2343	0.4877	-0.0283
	0.2	1.239	0.1824	0.6294	0.5637	0.7761	-0.2007
	0.7	1.3889	0.3321	1.1408	0.602	0.931	-0.3095
	Steady state	1.4247	0.3535	1.5254	0.6019	0.932	-0.3104
Pr	0.71	1.239	0.1824	0.6294	0.5637	0.7761	-0.2007
	2	1.1407	0.0228	0.5727	0.6172	0.7324	-0.1744
	7	1.077	2.41E-05	0.472	0.6176	0.6849	-0.157

https://doi.org/10.5281/zenodo.17252181

	0	1.2895	0.2624	0.7194	0.5477	0.7924	-0.2097
H	3	1.239	0.1824	0.6294	0.5637	0.7761	-0.2007
	5	1.2139	0.1445	0.5752	0.572	0.7671	-0.1958
	0.22			0.8867	0.7219	0.8617	-0.2568
Sc	0.6			0.6518	0.6189	0.7993	-0.2158
	0.75			0.6294	0.5637	0.7761	-0.2007
	0			0.6504	0.5056	0.7544	-0.1870
St	0.8			0.5664	0.7382	0.8413	-0.2417
	3			0.3354	1.3776	1.0801	-0.3922
	0			0.2110	0.6844	0.8082	-0.2175
K	3			0.8204	0.5132	0.7617	-0.1933
	5			1.1721	0.4276	0.7357	-0.1802

Table 2: Numerical comparison of Riemann sum approximation method (RSA) solutions, $PDEPE$ and steady state exact solutions $(ES)(Pr = 0.71, Sc = 0.60, H = 3, K = 2, N = 4, St = 0.2, \delta = 2)$

		Velocity				Velocity		
t	***r***	*RSA*	*PDEPE*	***t***	***r***	*RSA*	*PDEPE*	*ES*
0.2	1.2	0.1651	0.1657	0.6	1.2	0.2049	0.2055	
	1.4	0.1902	0.1903		1.4	0.2497	0.2499	
	1.6	0.1468	0.1467		1.6	0.2024	0.2023	
	1.8	0.076	0.0759		1.8	0.1084	0.1083	
0.4	1.2	0.1998	0.2004	1.6	1.2	0.2058	0.2065	0.2058
	1.4	0.2421	0.2423		1.4	0.2510	0.2514	0.2510
	1.6	0.1953	0.1952		1.6	0.2036	0.2037	0.2036
	1.8	0.1043	0.1041		1.8	0.1091	0.1091	0.1091

https://doi.org/10.5281/zenodo.17252181